BMC Biology

RESEARCH

Open Access

Transcriptome analysis reveals PTBP1 as a key regulator of circRNA biogenesis

Mohan Wang[1,2†], Shanshan Zheng[2†], Yan Zhang[1,2], Jingwen Zhang[1,2], Fuming Lai[2], Cong Zhou[1,2], Qiangwei Zhou[1,2], Xingwang Li[1] and Guoliang Li[1,2*]

Abstract

Background Circular RNAs (circRNAs) are a class of non-coding RNAs generated through back splicing. High expression of circRNAs is often associated with numerous abnormal cellular biological processes. However, the regulatory factors of circRNAs are not fully understood.

Results In this study, we identified PTBP1 as a crucial regulator of circRNA biogenesis through a comprehensive analysis of the whole transcriptome profiles across 10 diverse cell lines. Knockdown of PTBP1 led to a significant decrease in circRNA expression, concomitant with a distinct reduction in cell proliferation. To investigate the regulatory mechanism of PTBP1 on circRNA biogenesis, we constructed a minigene reporter based on *SPPL3* gene. The results showed that PTBP1 can bind to the flanking introns of circ*SPPL3*, and the mutation of PTBP1 motif impedes the back splicing of circ*SPPL3*. Subsequently, to demonstrate that this observation is not an exception, the comprehensive regulatory effects of PTBP1 on circRNAs were confirmed by miniGFP, reflecting the necessity of the binding site in the flanking introns. Analysis of data from clinical samples showed that both PTBP1 and circRNAs exhibited substantial upregulation in acute myeloid leukemia, further demonstrating a potential role for PTBP1 in promoting circRNA biogenesis under in vivo conditions. Competitive endogenous RNA (ceRNA) network revealed that PTBP1-associated circRNAs participated in biological processes associated with cell proliferation.

Conclusions In summary, our study is the first to identify the regulatory effect of PTBP1 on circRNA biogenesis and indicates a possible link between PTBP1 and circRNA expression in leukemia.

Keywords Circular RNAs, RNA binding proteins, PTBP1, Transcriptome, Biogenesis

†Mohan Wang and Shanshan Zheng contributed equally to this work.

*Correspondence:
Guoliang Li
guoliang.li@mail.hzau.edu.cn
Full list of author information is available at the end of the article

Graphical Abstract

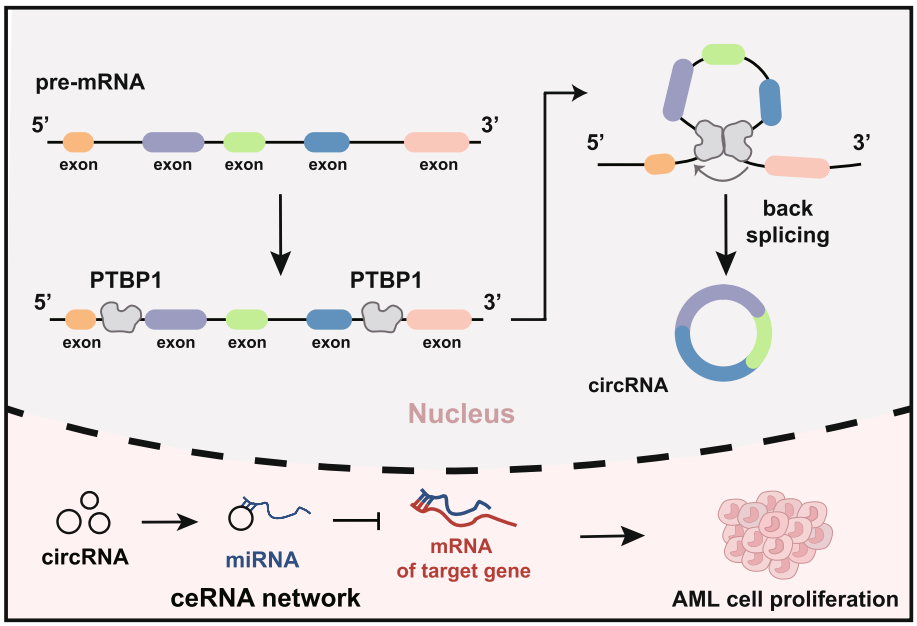

Background

An RNA molecule, lacking polyadenylation and exhibiting exon disorder, was uncovered in the 1970 s, later recognized as circRNA [1, 2]. With the remarkable advancements in RNA sequencing technology and the emergence of bioinformatics, the exploration of circRNAs has undergone a remarkable surge. Nevertheless, there remains an urgent necessity for further investigation to fully understand the intricate interactions of circRNAs with other molecules and to unravel the complex mechanisms of their biogenesis.

It was demonstrated that circRNAs are generated through back splicing, forming stable covalent closed structures [3]. CircRNAs predominantly reside in the cytoplasm or exosomes, exhibiting distinctive features such as tissue-specificity, disease-specificity, and high stability. CircRNAs encompass various biological functions, with a key role as miRNA sponge [4]. More precisely, circRNAs abundant with miRNA response elements can prevent the interactions between mRNA and miRNA and consequently indirectly regulate the expression of target genes [5, 6].

CircRNAs have three primary modes of biogenesis [7]. The initial mode involves circRNA generation through splicing on the pre-mRNA, achieved by the sequential assembly of snRNP, catalyzing the joining of the 5′ donor site of the exon to the 3′ acceptor site [8]. The second mode involves certain circRNAs containing reverse complementary matches (RCMs) in their flanking introns, forming double-stranded RNAs at splice sites and producing circRNAs through alternative splicing. It is noteworthy that short reverse complementary matches can effectively promote cyclization [9]. Nonetheless, the presence of reverse complementary sequences in the flanking introns alone does not guarantee circRNA production, as various other factors also influence circRNA formation. The third mode relies on RNA binding proteins (RBPs) to promote cyclization. It has been confirmed that several RBPs, including QKI, Mbl, FUS, NOVA2, ADAR, HNRNPM, and HNRNPL, play a crucial role in regulating circRNA biogenesis [10–16]. It is not clear whether there are other RBPs important in circRNA biogenesis.

In this study, we analyzed circRNAs from 10 cell lines and found that the motifs of RNA binding protein PTBP1 were enriched in the flanking regions of circRNAs. The knockdown of PTBP1 led to remarkable downregulation of the global circRNA level in K562 cells. These changes in circRNA expression were largely independent from linear transcriptional changes of the host genes. The regulation of circRNA biogenesis by PTBP1 was additionally validated using PTBP1 RIP-seq and a minigene reporter. Importantly, it was revealed that PTBP1 binding on the intronic sequences on both sides of the circRNAs played a crucial role in their back splicing. RNA-seq data from clinical samples of acute

myeloid leukemia (AML) patients disclosed a significant upregulation of PTBP1 and global circRNA levels, further demonstrating an association of PTBP1 expression and circRNA biogenesis under in vivo conditions. Simultaneously, PTBP1-associated ceRNA network showed that differentially expressed circRNAs with the highest network connectivity may constitute the core of the regulatory network and are closely linked to AML malignant proliferation.

Results

PTBP1 was identified as the top pivotal RBPs governing circRNAs

To investigate the profile of global circRNA expression, we collected public transcriptome datasets from 10 cell lines in ENCODE project. Through analysis of the identified circRNAs, we discovered a notable cell specificity in circRNA expression, with over 25% of circRNAs being unique to individual cell lines (Fig. 1A, Additional file 2:

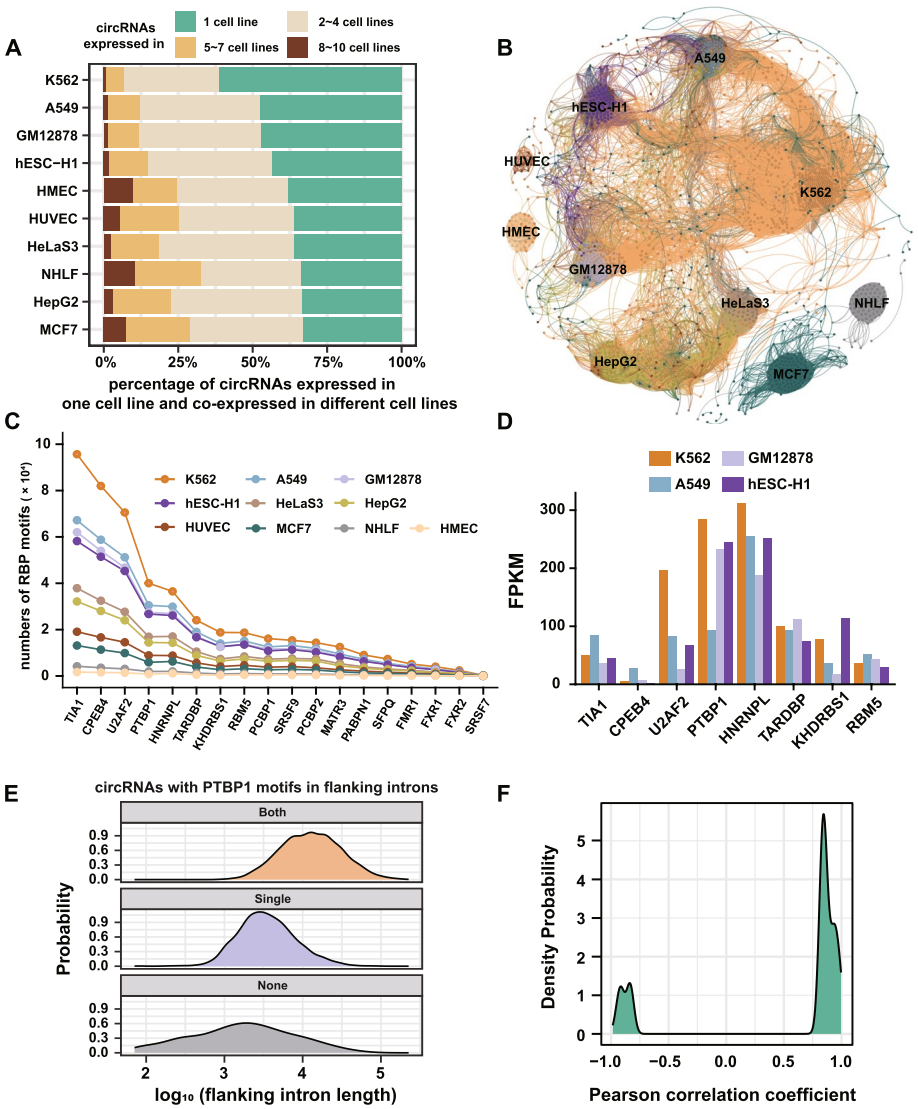

Fig. 1 PTBP1 was screened as a key RBP for the regulation of circRNA. **A** CircRNAs identified from 10 cell lines in ENCODE project and co-expressed in other cell lines. Different colors represent circRNAs expressed in 1, 2 ~ 4, 5 ~ 7, and 8 ~ 10 cell lines, respectively. **B** CircRNA co-expression networks. Each node represents a circRNA, and the node color indicates the cell line with the highest expression level of the circRNA. Each edge represents the Pearson correlation coefficient greater than 0.9 between two circRNAs. **C** Numbers of RBP motifs in circRNA flanking introns in 10 cell lines. The x-axis represents different RBPs. Different colors of the lines represent different cell lines. **D** Gene expression levels of the top RBPs with the largest numbers of motifs. FPKM was obtained from the ENCODE project. Four cell lines with the largest numbers of RBP motifs were demonstrated. **E** Length distribution of circRNA flanking introns identified in K562 cell line with or without the PTBP1 motifs. **F** Pearson correlation coefficient between PTBP1 and circRNAs across 10 cell lines

Table S1). By constructing an elaborate co-expression network for circRNAs, it was observed that the correlations at the nodes of the network effectively distinguished between different cell types (Fig. 1B). This implies that both the nodes and the edges within the network exhibited distributions that were specific to particular cell lines. Collectively, these findings underscore the robust cell specificity inherent in circRNA expression profiles.

To identify RBPs critically involved in circRNA regulation, we analyzed the motifs of RBPs in 10 cell lines. Notably, many RBPs showed the large numbers of motifs in the flanking introns of circRNAs in K562 cells (Fig. 1C). PTBP1 and HNRNPL exhibited the highest expression levels among the top 8 RBPs with the largest numbers of motifs (Fig. 1C, D). Since one existing study has reported on the regulatory role of HNRNPL in circRNA biogenesis [16], we have opted to focus our research on PTBP1. To further elucidate the effect of PTBP1 on circRNAs, we delved into the length distribution of the flanking introns of circRNAs. Our analysis revealed that the flanking introns of circRNAs harboring PTBP1 motifs were considerably longer, a finding that sets them apart from those without such motifs (Fig. 1E). We conducted an analysis of the correlation distributions between PTBP1 and circRNAs, revealing a robust positive correlation between the expression levels of circRNAs and PTBP1 (Fig. 1F). This significant association implies that PTBP1 likely exerts a crucial role in regulating the levels of circRNAs. Taken together, we found that PTBP1 was abundant in K562 cells and its motifs were enriched in the flanking introns of circRNAs, demonstrating that PTBP1 may be an essential circRNA regulator.

Knockdown of PTBP1 in K562 cells decreases global circRNA levels and affects cell proliferation

To explore the impact of PTBP1 on circRNA biogenesis, we knockdown PTBP1 in K562 cell line (Additional file 1: Fig. S1 A, B) and generated circRNA-seq data from wild-type and PTBP1-knockdown cell lines. The circRNA-seq libraries were constructed by digestion with RNase R exonuclease to eliminate the interference of linear products. Then, circRNA identification was accomplished by scanning the back splicing junction sequences using CIRIquant and CIRCexplorer2 software. The subsequent analyses focused on exon-compositional circRNAs co-identified by both software packages. Specifically, the K562 wild-type libraries identified 7647 circRNAs, while the two knockdown cell lines identified 4944 and 5227 circRNAs, respectively (Fig. 2A, Additional file 2: Table S1). The counts per million (CPM) of circRNAs in the knockdown group (shP1 and shP2) was significantly decreased compared to the wild-type (WT) group (Fig. 2B, Additional file 3: Table S2, Additional file 4: Table S3).

To enhance reliability, we identified 49 overlapping differentially expressed circRNAs in both knockdown groups. The analysis revealed that the majority of differentially expressed circRNAs were significantly downregulated, and this trend was consistent in both knockdown groups (Fig. 2C). To investigate the changes in linear transcripts, we analyzed the differential expression of all linear transcripts using RNA-seq data (Additional file 5: Table S4). The volcano plot reveals that there are differentially expressed linear mRNAs (Additional file 1: Fig. S2 A). However, the number of such differentially expressed linear mRNAs is small when compared to total number of linear mRNAs. Importantly, the abundance of linear mRNAs corresponding to differentially expressed circRNAs has not undergone significant changes (Additional file 1: Fig. S2 A). Meanwhile, the density scatter plot of the knockdown groups, K562-shP1, demonstrated a significant downward shift in circRNAs abundance along the vertical direction, whereas the corresponding linear transcripts abundance did not exhibit a significant shift horizontally (Fig. 2D). Similar results were observed for the other knockdown group, K562-shP2 (Additional

(See figure on next page.)

Fig. 2 PTBP1 regulates circRNA biogenesis and affects the cell proliferation of K562 cells. **A** Genome-wide distribution of all circRNAs identified in wild-type (WT), shPTBP1-1 (shP1), and shPTBP1-2 (shP2) conditions (labeled with blue, gray, and yellow lines, respectively). The y-axis represents the average counts per million mapped reads (CPM) in the range of 0–1. Some genomic regions of circRNAs with expression changes are marked by red background. **B** Boxplot illustrating the expression levels of all the circRNAs identified in the WT, shP1, and shP2 groups. **C** The pie chart depicts the number and proportion of circRNAs differentially expressed (DE) in either shP1 or shP2 group, or both groups. The heatmap indicates the expression levels of circRNAs that were differentially expressed in both groups. Color bar represents the *z*-score of circRNA expression levels. **D** The density scatter plot reflects the Pearson correlation of fold change of expression levels from circRNAs and the corresponding linear transcripts identified in WT-shP1 group. **E** Fold change of expression levels of 10 selected circRNAs and corresponding linear transcripts from RT-qPCR in WT-shP1 group. $n = 3$ biological replicates. Error bars are represented as mean ± standard error of means (SEM). * $p < 0.05$; ** $p < 0.01$; *** $p < 0.001$; ns, not significant. Student's *t*-test was used for statistical significance test (two-tailed, unpaired). **F** Correlation of fold change of expression levels from transcriptome sequencing data and RT-qPCR data in WT-shP1 group. The gray areas represent 95% confidence intervals. The *R*-squared value (R^2) is shown in the upper left corner, representing the interpretability of the linear model, and indicating strong correlation between transcriptome and RT-qPCR result in circRNA and corresponding linear mRNA analysis. **G** Fold change of cell numbers over 7 days in K562 wild-type and knockdown cell lines. *** $p < 0.001$

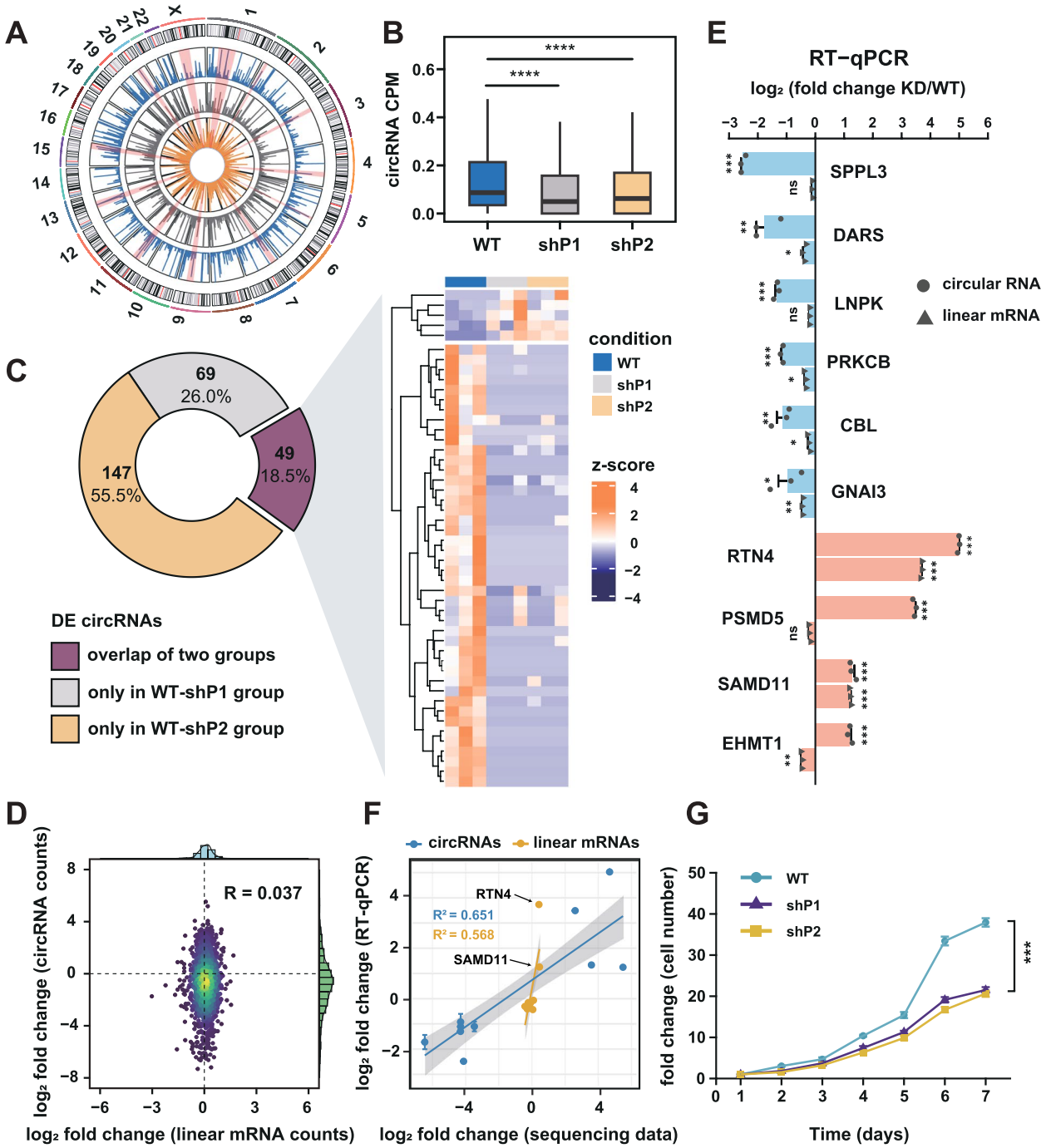

Fig. 2 (See legend on previous page.)

file 1: Fig. S2B), suggesting that the regulation of these differentially expressed circRNAs by PTBP1 is independent of the process of splicing of their pre-mRNAs to generate linear transcripts.

To further validate the differentially expressed circRNAs and their corresponding linear transcripts, we performed RT-qPCR amplification on 10 selected circRNAs in two knockdown cell lines. Considering the levels of differential expression and the challenges in designing specific primers, we ultimately selected top 6 downregulated and 4 upregulated circRNAs for examination (Fig. 2E, Additional file 1: Fig. S2 C, Additional file 6: Table S5). Correlation analysis revealed that the transcriptomic data were consistent with the RT-qPCR results, except for the

linear transcripts of circ*RTN4* and circ*SAMD11* (Fig. 2F, Additional file 1: Fig. S2D). Furthermore, we observed a drastic decrease in the proliferative ability of K562 after knockdown of PTBP1 (Fig. 2G), indicating that PTBP1 may be essential for cell proliferation.

The regulation of circRNAs by PTBP1 is cell-type specific

To investigate the impact of PTBP1 on circRNA biogenesis across different cell types, we downloaded two public datasets and analyzed circRNA expression in two cell types after PTBP1 knockdown. CD34 + cells had low circRNA expression, and global circRNA expression did not change greatly (Additional file 1: Fig. S3 A). The density scatter plot of the knockdown group showed that the abundance of circRNAs and linear transcripts did not shift significantly in their respective axes (Additional file 1: Fig. S3 C). Despite this, a differential expression analysis revealed that in CD34 + cells, there were 227 circRNAs downregulated and 174 circRNAs upregulated, respectively (Additional file 1: Fig. S3E).

In contrast, circRNA abundance in HeLa cells was significantly upregulated (Additional file 1: Fig. S3B), with 263 circRNAs downregulated and 603 circRNAs upregulated (Additional file 1: Fig. S3 F). Nonetheless, the abundance of linear transcripts corresponding to these circRNAs experienced a decline, as shown by the density scatter plots (Additional file 1: Fig. S3D). In these two cell types, the expression levels of circRNAs exhibit an extremely weak positive correlation and a negative correlation with linear transcripts, respectively (Additional file 1: Fig. S3 C, D). This indicates that these circRNAs are regulated independently from the mRNAs also deriving from the host genes. Overall, the regulatory role of PTBP1 in circRNA biogenesis may be cell-specific.

Characterization and identification of circ*SPPL3* as the target of PTBP1

We analyzed the junction ratio of 49 overlapping differentially expressed circRNAs (Fig. 2C and D) in the two PTBP1 knockdown groups and found that circ*SPPL3* not only possessed a high junction ratio ranking (Additional file 1: Fig. S4 A, Additional file 7: Table S6), but also showed the most significant reduction in expression (Fig. 2E).

Subsequently, we proceeded with the biological identification of circ*SPPL3*. Circ*SPPL3* spans 1939 bp (Chr12:120,782,655–120784593) and originates from back splicing of exons 4–6 of the *SPPL3* gene (Additional file 1: Fig. S4B). Primers were designed for the back splicing junction site of circ*SPPL3*, and PCR amplification was performed using cDNA as a template, which was identified by Sanger sequencing (Additional file 1: Fig. S4 C). Digestion of circ*SPPL3* using RNase R exonuclease demonstrated that circ*SPPL3* was more tolerant than linear RNA (Additional file 1: Fig. S4D). We designed convergent and divergent primers to identify circ*SPPL3*, and the results showed that the target bands could be amplified (Additional file 1: Fig. S4E, F).

PTBP1 governs the back splicing of circ*SPPL3* via recognition of flanking intron motifs

To explore the characteristics of PTBP1 binding to RNA, we generated RIP-seq data for PTBP1. From 252,221,548 clean reads, we identified 20,156 peaks and found that PTBP1 mainly binds to introns (47.31%) and promoters (37.36%) (Fig. 3A). Enrichment of PTBP1 binding sequences using HOMER software revealed that the motifs were primarily UC repeats (Fig. 3B), consistent with previous reports [17]. PTBP1 binding profiles upstream and downstream of back splicing junction sites were analyzed separately, revealing significant differences between the enrichment of differentially expressed circRNAs and all circRNAs. In differentially expressed circRNAs, the binding profiles of PTBP1 were mainly enriched in introns adjacent to the back splicing junction sites, but it was not observed in all circRNAs (Fig. 3C). Meanwhile, we examined the expression of circRNAs with different binding conditions and found that the expression of circRNAs with PTBP1 binding in the flanking introns was significantly higher than circRNAs without PTBP1 binding in the flanking introns (Fig. 3D).

To determine the specific regulatory site of PTBP1 on circ*SPPL3*, we examined the binding of PTBP1 in the flanking introns of circ*SPPL3* (Fig. 3E). To facilitate the subsequent validation of these regulatory sites, we constructed a minigene reporter. According to previous reports, mutating UYYY to CCCC can effectively prevent PTBP1 binding [18]. Multiple UYYY motifs were found by scanning the circ*SPPL3* flanking sequences (Fig. 3F). To assess the effect of PTBP1 binding, we first mutated one RIP peak motif and two non-RIP peak motifs (Mt1) located upstream. The relative quantification of circ*SPPL3* using RT-qPCR revealed that PTBP1-mediated back splicing of circ*SPPL3* was significantly decreased compared to the wild type. We subsequently mutated three non-RIP peak motifs (Mt2) located upstream. Interestingly, these motifs, although lacking PTBP1 RIP support, also showed similar results to Mt1. Mutating one RIP peak motif and two non-RIP peak motifs downstream (Mt3) was found to also reduce PTBP1-mediated back splicing of circ*SPPL3* (Fig. 3G). Our data indicates that destroying the binding sites of PTBP1 on either side of the intron of circ*SPPL3* locus was able to inhibit its regulatory effects.

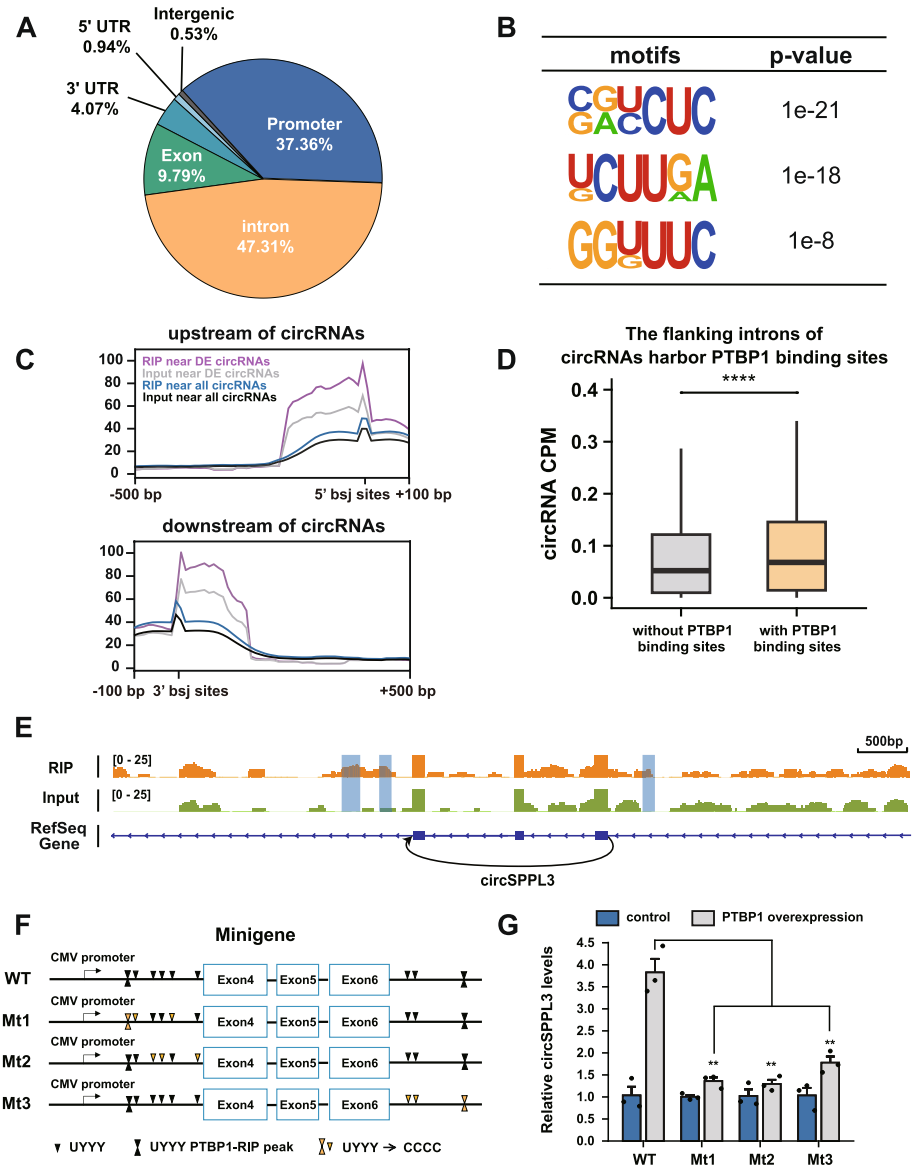

Fig. 3 Characterization of PTBP1 binding sites in flanking introns and the effects on circRNA expression. **A** Pie chart shows the distribution of PTBP1 RIP peaks in different genomic regions. **B** Motifs and *p* values enriched from PTBP1 RIP peaks are shown. **C** Profile of PTBP1 RIP-seq and input near the back splicing junction sites of all circRNAs and differentially expressed circRNAs. **D** The expression level of circRNAs with and without PTBP1 binding sites in flanking introns in K562 WT cell line. **E** Distribution of PTBP1-bound signals within 3 kb upstream and downstream of circ*SPPL3* was demonstrated by the Integrative Genome Browser. Blue squares mark the PTBP1 binding regions on introns. **F** Minigene reporter schematics for circ*SPPL3*. The PTBP1-RIP peak motif is represented by two black triangular symbols, motifs unrelated to the PTBP1-RIP peak are represented by one black triangular symbol, and yellow triangular symbols indicates that the motif is mutated. **G** RT-qPCR quantification of circ*SPPL3* from minigene reporters co-transfected with PTBP1 expression plasmid (PTBP1-overexpression) or empty vector in 293 T cells. Linear transcript generated from the reporter was used for normalization. $n = 3$ biological replicates. Error bars are represented as mean ± standard error of means (SEM). * $p < 0.05$, ** $p < 0.01$, Student's *t*-test, two-tailed and unpaired

The presence of PTBP1 binding sites in flanking introns facilitates circRNA biogenesis

MiniGFP was utilized as a model to validate circRNA biogenesis in previous study [19]. This system splits *EGFP* gene into two parts and inserts them into the vector in reverse order. The reverse complementary matches (RCMs) on both sides of *EGFP* promote its cyclization, allowing the expression of green fluorescent proteins after the formation of circRNAs. To further confirm that the binding of PTBP1 upstream and downstream of the cyclization site can effectively promote circRNA biogenesis, we inserted UYYY motif sequences upstream

and downstream of this model (Fig. 4A). Fluorescence was generated after transient transfection of miniGFP (Fig. 4B), and circ*GFP* bands amplified from RT-PCR were resistant to digestion with RNase R exonuclease, while *GAPDH* bands were degraded as expected (Fig. 4C).

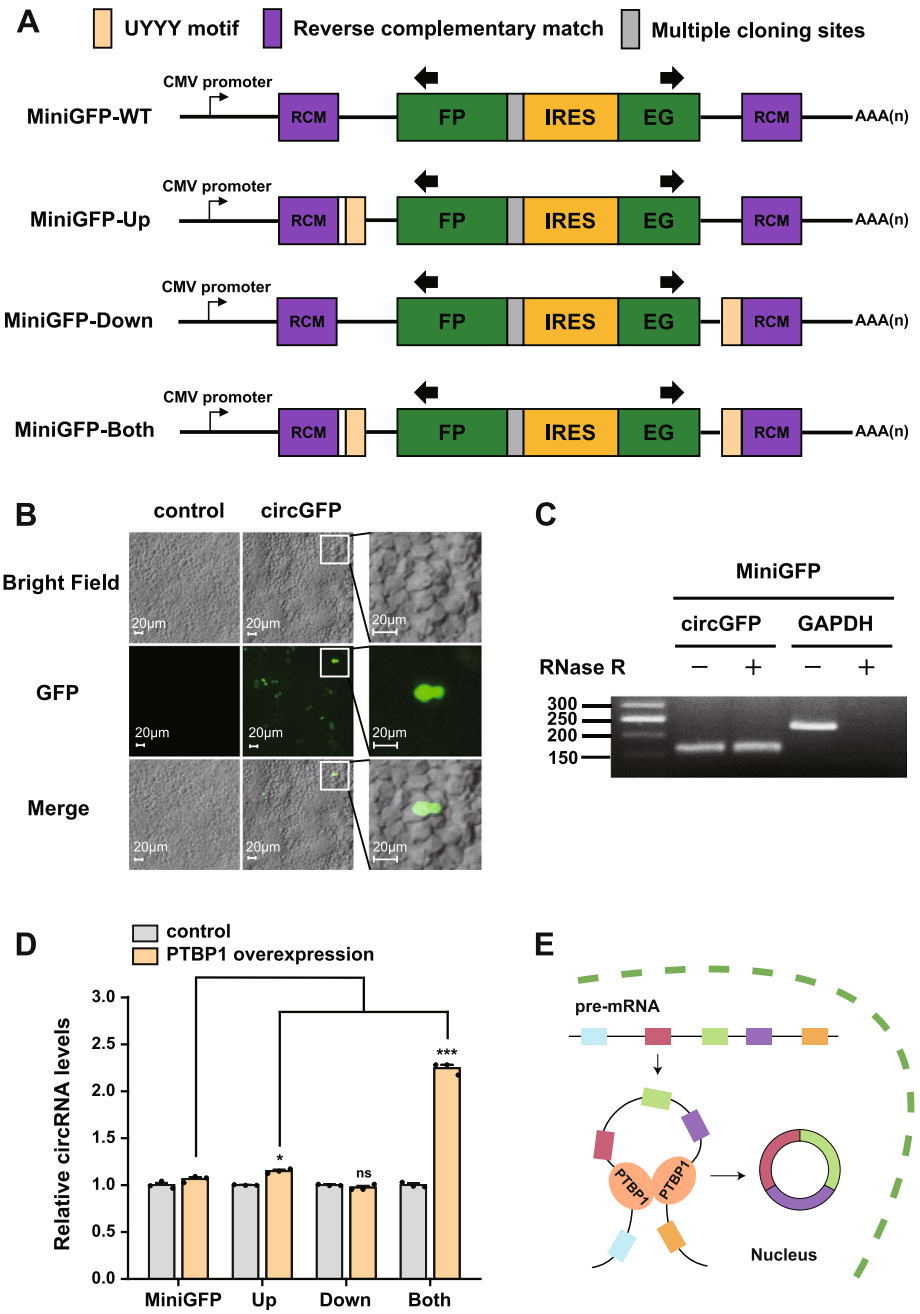

Fig. 4 Coexistence of PTBP1 binding sites on both sides of the introns induces pre-mRNA back splicing. **A** Schematic representation of the miniGFP construct used to validate circRNA biogenesis. Green squares represent the *EGFP* gene that was split into two parts. Reverse complementary matches (RCMs) and internal ribosome entry sites (IRES) are shown as purple and golden squares, respectively. Yellow squares represent UYYY motifs inserted into introns. **B** Fluorescence after transient transfection of miniGFP. **C** RT-PCR detection of the circ*GFP* and *GAPDH* with or without RNase R exonuclease treatment. **D** RT-qPCR quantification of circ*GFP* from miniGFP co-transfected with PTBP1 expression plasmid (PTBP1-overexpression) or empty vector in 293 T cells. Linear transcript generated from the reporter was used for normalization. $n = 3$ biological replicates. Error bars are represented as mean ± standard error of means (SEM). * $p < 0.05$; *** $p < 0.001$; ns, not significant, Student's *t*-test, two-tailed and unpaired. **E** Schematic representation of PTBP1 participating circRNA biogenesis by binding in circRNA flanking introns

In the miniGFP system devoid of the UYYY motif, it was observed that PTBP1 failed to induce an increase in back splicing events leading to circ*GFP* (Fig. 4D). Upon insertion of a 10 × UYYY motif either upstream (Up) or downstream (Down) of miniGFP, the results are the same with the wild type and did not facilitate circ*GFP* biogenesis. Coexistence of upstream and downstream PTBP1 binding sites (Both) resulted in a significant increase in circ*GFP* production compared to the wild type through co-transfection with PTBP1 (Fig. 4D, Additional file 6: Table S5). We found that effective promotion of circRNA biogenesis is achievable only when PTBP1 binding sites are concurrently present on both sides of the circRNA locus (Fig. 4E).

PTBP1 is simultaneously upregulated with circRNAs in AML

To determine whether PTBP1 exerts its regulatory influence through a conserved mechanism under in vivo conditions, we collected a dataset of acute myeloid leukemia (AML) clinical samples from the GEO database. Significant upregulation of PTBP1 was observed in AML compared to healthy samples (Fig. 5A). AML patients with higher PTBP1 expression level experienced notably lower survival rates compared to those with lower PTBP1 expression level, which indicates a potential contribution of increased PTBP1 expression to the progression of AML (Fig. 5B). At the same time, the global circRNA levels showed a significant upregulation in AML (Fig. 5C), and the density scatter plot indicated a significant upward shift in circRNAs expression along the vertical direction, whereas linear transcripts expression did not exhibit a significant shift along the horizontal direction (Fig. 5D). More than 70% of differentially expressed circRNAs may have PTBP1 motifs on both sides of the introns (Additional file 1: Fig. S5 A). Additionally, similar to previous results in K562 cells (Fig. 2C, E), circ*SPPL3* expression was significantly upregulated in AML compared to the healthy group, consistent with the trend observed for PTBP1. The junction ratio ranking of circ*SPPL3* in AML was relatively high (Fig. 5E, F). Our preliminary observations indicate that PTBP1 could potentially influence circRNA biogenesis in AML cells, with a tentative association observed in prognostic analyses [20].

PTBP1 may influence cell proliferation in AML through the regulation of circRNAs

Acute myeloid leukemia represents a myeloid-origin malignant hematological disease characterized by rapid onset. Development of innovative therapies has contributed to an increase in the average 5-year relative survival rate for leukemia. However, in developing countries like China, the survival rate remains considerably low [21].

To further explore whether PTBP1 is associated with AML progression, we conducted gene set enrichment analysis (GSEA) on 961 differentially expressed genes between healthy and AML samples. The results revealed that these genes were involved in endothelial cell proliferation, endothelial cell metastasis, and mRNA splicing (Fig. 6A–C).

To elucidate the connection between these differentially expressed genes and differentially expressed circRNAs, we constructed a ceRNA network. We screened differentially expressed circRNAs with PTBP1 motifs and focused on 471 target differentially expressed genes regulated by these circRNAs. Gene ontology (GO) analysis of these target genes revealed that their cellular components predominantly included the plasma membrane, extracellular exosome and focal adhesion, etc. The molecular functions encompassed protein homodimerization activity, receptor binding and protein kinase binding, etc. Biological processes included positive regulation of B cell proliferation, MAP kinase activity, ERK1 and ERK2 cascade, PKB signaling, and cell proliferation (Fig. 6D). The KEGG pathway analysis revealed predominant involvement in the FoxO signaling pathway, MAPK signaling pathway, Rap1 signaling pathway, Ras signaling pathway, and TGF-β signaling pathway (Fig. 6E), which have been proven to be associated with cell proliferation [22–26].

A previous study has confirmed that PTBP1 can promote the proliferation of AML cells [27], but the underlying mechanisms have not been elucidated. To explore the potential targets through which PTBP1 enhances cell proliferation in AML, we conducted a screening within the ceRNA network. In the cell proliferation-related ceRNA network ranked according to the degree of connectivity, circ*FNDC3B*, circ*ABCC1*, circ*RNF13*, circ*PRKCB*, circ*ITPR2*, and circ*AGTPBP1* were identified as potential hub circRNAs in this regulatory network (Fig. 6F). Our study identified 78 miRNAs, including *miR-1236-3p*, *miR-1248*, and *miR-3065-5p*, as potentially residing at critical nodes within the regulatory network, under the influence of these pivotal hub circRNAs (Fig. 6F, Additional file 8: Table S7). These preliminary observations hint at the possibility that PTBP1 might have an association on cell proliferation in AML samples, potentially through modulation of the expression levels of certain core circRNAs when interacted with miRNAs.

Discussion

In the literature, PTBP1 has been shown to be able to influence gene expression by regulating alternative splicing [28]. Nevertheless, the molecular mechanism of PTBP1 regulating global circRNA biogenesis is not reported. We found that depletion of PTBP1 in K562 cells led to a reduction in global circRNA levels,

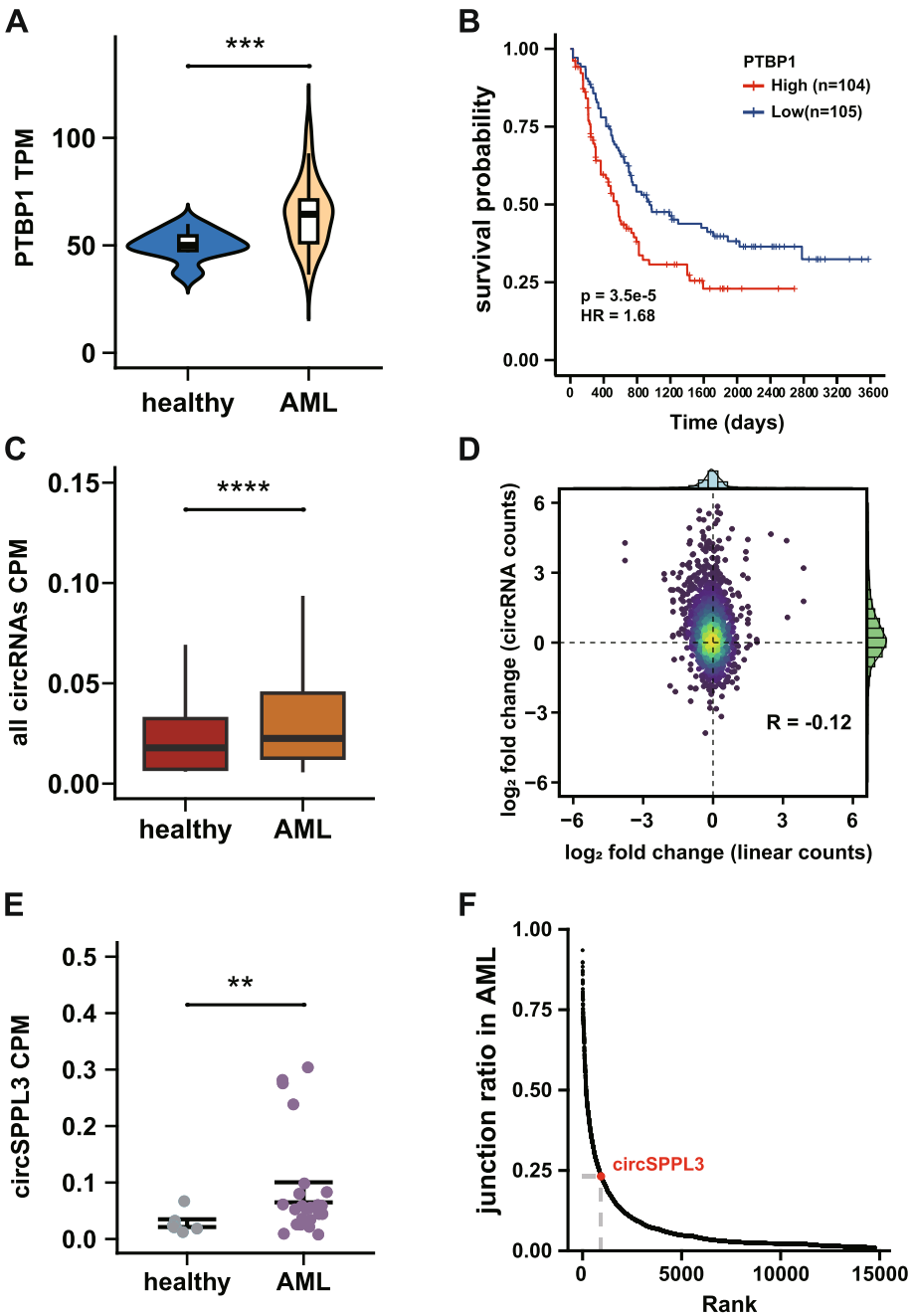

Fig. 5 PTBP1 is simultaneously upregulated with circRNAs in AML and associated with poor prognosis. **A** Violin plot demonstrates the PTBP1 expression levels in healthy and AML samples. RNA-seq data for healthy and AML tissues were obtained from GSE158596. **B** Kaplan–Meier analysis of overall survival for AML patients with PTBP1 from TCGA and TARGET database. Red and blue curves represent the survival of AML patients with higher and lower PTBP1 expression levels, respectively. HR, hazard ratio. **C** Boxplot shows the expression levels of all circRNAs in healthy and AML samples. **D** Density scatter plot reflects the correlation of fold change of expression levels from circRNAs and the corresponding linear transcripts identified in AML versus healthy samples. **E** Circ*SPPL3* expression levels in healthy and AML samples. **F** Junction ratio of circRNAs in AML calculated by CIRIquant software

with no significant change in the corresponding linear transcripts. This indicates that the regulatory impact of PTBP1 on circRNAs is irrelevant to the linear transcripts splicing, although PTBP1 has functions in alternative splicing. Through the analysis of differentially expressed circRNAs after PTBP1 depletion, we identified circ*SPPL3*

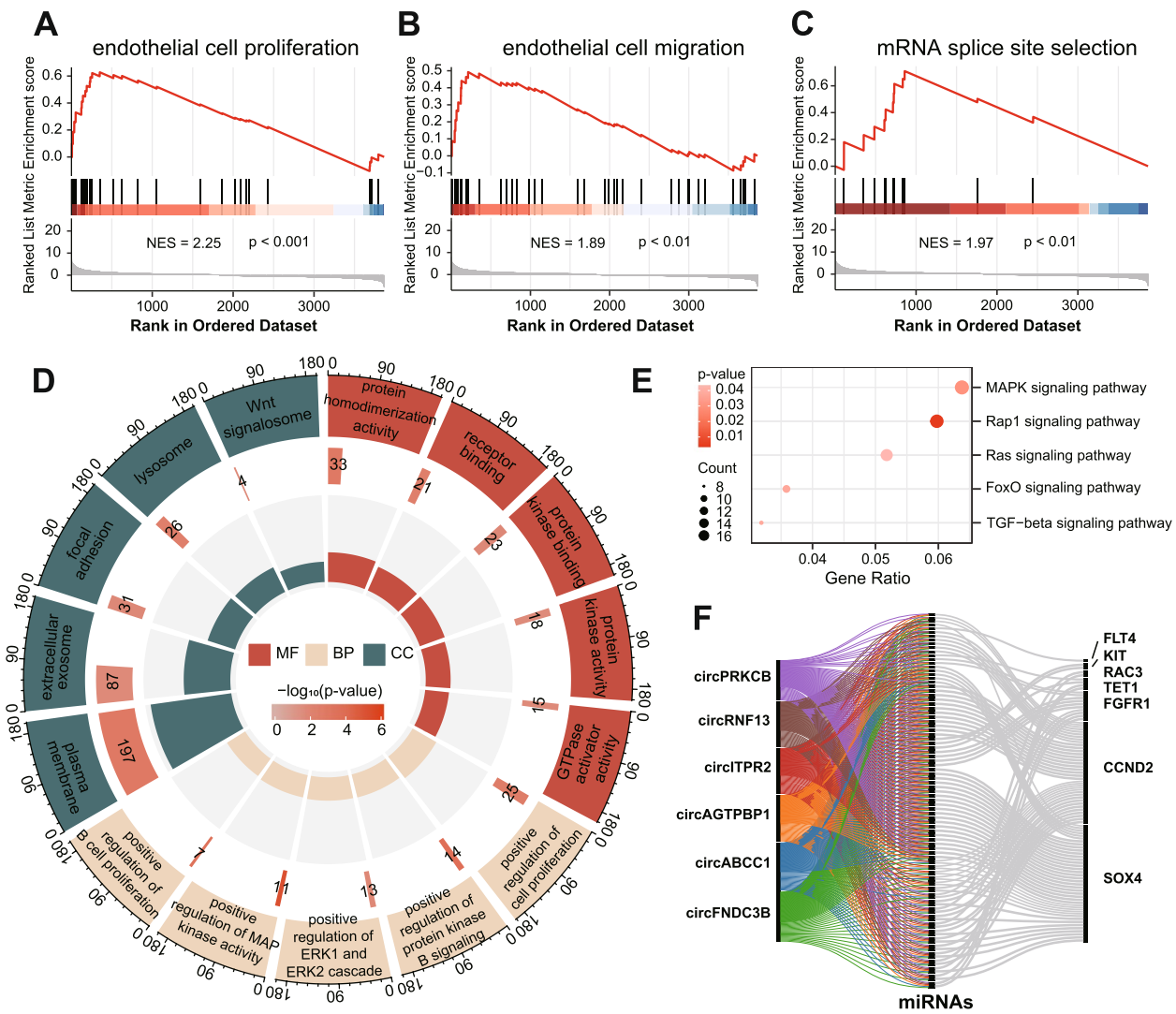

Fig. 6 PTBP1-related circRNAs are associated with cell proliferation in AML. **A**–**C** Gene set enrichment analysis (GSEA) shows the significant pathway enriched in differentially expressed genes in AML. Normalized enrichment score (NES) reflects the enrichment level of differentially expressed genes associated with specific pathway relative to all differentially expressed genes. **D** GO enrichment of differentially expressed genes in ceRNA network. The outer circle represents 15 GO terms enriched in MF, BP, and CC. The middle circle represents the number of differentially expressed genes enriched in the corresponding GO terms, with the color representing the significance of the enrichment. The inner circle represents the gene ratio. **E** Dot plot shows five KEGG pathways enriched with differentially expressed genes in ceRNA network. **F** CeRNA networks of six hub circRNAs associated with cell proliferation

as a potentially crucial target of PTBP1 regulation and discovered that PTBP1 can regulate the biogenesis of circ*SPPL3* by binding to intronic sequences on both sides using a minigene reporter. Expression levels of both PTBP1 and circRNAs were significantly upregulated in AML samples. Patients exhibiting high expression of PTBP1 experienced a poorer prognosis. The ceRNA network indicated that PTBP1 and hub circRNAs might be involved in the regulation of cell proliferation in AML.

CircRNAs generally exhibit lower expression compared to linear RNAs, and lowly expressed circRNAs may be undetected, which brings challenges in circRNA identification. To enhance circRNA enrichment before RNA library construction, we employed RNase R exonuclease to effectively minimize the interference from linear RNA. Additionally, we employed two circRNA identification software to reduce the false positive (Additional file 3: Table S2). The partially differentially expressed circRNAs were validated using RT-qPCR (Fig. 2E). Employing higher-precision methods, such as third-generation sequencing technology [29], has the potential to significantly enhance validation efficiency.

The binding sites of RBPs on the flanking introns of circRNAs are crucial for regulating the biogenesis of circRNAs. We discovered that the expression levels of circ*SPPL3* in the K562 cell line are notably high and are not influenced by the expression levels of its corresponding linear mRNA (Additional file 1: Fig. S4 A, Additional file 7: Table S6) [30]. The downregulation of circ*SPPL3* is most significant after the knockdown of PTBP1 (Fig. 2E). We validated circ*SPPL3* in K562 cells (Additional file 1: Fig. S4D) and analyzed the binding characteristics of PTBP1 in the flanking introns of the regulated circRNAs. We found that the motif of PTBP1 was characterized by UYYY (Fig. 3B). Not all PTBP1 motifs are supported by RIP-seq data, suggesting that although RIP-seq data is an essential guide for detecting key binding sites of RBPs, its role in predicting crucial binding sites for back splicing may be limited. Through the construction of a minigene reporter and different mutants for circ*SPPL3*, we found that the motifs in its flanking introns are essential for the regulation of PTBP1 (Fig. 3G). This may indicate that the simultaneous retention of PTBP1 motifs in both introns is necessary for circRNA biogenesis.

In various types of leukemia, abnormal gene splicing frequently occurs due to genetic mutations and other factors [31, 32]. This aberrant genetic splicing typically results in different exon combinations and contributes to the heterogeneity of cancer cells. We observed a significant upregulation of both PTBP1 and circRNA expression in AML samples compared with healthy samples (Fig. 5A, C). We also found a higher number of significantly upregulated circRNAs with high junction ratio in AML (Additional file 1: Fig. S5B), such as circ*IRAK3*. Meanwhile, the high expression of PTBP1 is associated with the low survival rate of AML patients (Fig. 5B), highlighting the need for further experimental validation of its impact on leukemia progression.

Through the establishment of a ceRNA network associated with PTBP1, we identified that the majority of target genes regulated by PTBP1 through the ceRNA network were involved in cell proliferation (Fig. 6D, E). This observation suggests that PTBP1 may promote cell proliferation in AML, aligning with the findings of previous report [27]. In the cell proliferation-related networks, we identified six hub circRNAs with the highest connectivity (Fig. 6F). Circ*FNDC3B* [33], circ*ABCC1* [34, 35], circ*RNF13* [36–38], and circ*AGTPBP1* [39], which differentially express between healthy and AML samples, have been discovered to be associated with the progression of various cancers. Although circ*ITPR2* has been rarely reported, *ITPR2* promotes the proliferation of hepatocellular carcinoma cells and it has been shown to be a key gene in prostate cancer prognosis [40, 41]. Circ*PRKCB* also exhibited significant differential expression in our K562 data (Fig. 2E), and the trend of change was consistent with PTBP1, suggesting that it is conserved and plays a crucial role in multiple types of leukemia. In summary, the findings indicate that the proliferation of AML cells may be linked to the expression of these hub circRNAs and PTBP1, and additional wet lab experiments are necessary to elucidate their regulatory interactions in the future.

Conclusions

In this study, PTBP1 was initially identified as a pivotal regulator of circRNAs through the analysis of transcriptomic data across 10 distinct cell lines. The knockdown of PTBP1 in K562 cells led to a significant reduction in the overall abundance of circRNAs. Subsequently, we employed a minigene reporter and a miniGFP system to substantiate the molecular mechanism, underlying PTBP1's role in promoting global circRNA biogenesis. Further analysis of data from acute myeloid leukemia patient samples indicated the view that PTBP1 potentially functions as a key regulator of circRNAs under in vivo conditions. Additionally, we explored the potential involvement of PTBP1-associated circRNAs in biological processes pertinent to cellular proliferation. This is the first report to describe the role of PTBP1 in regulating global circRNA biogenesis. Our findings suggest that circRNAs associated with PTBP1 could play a role in cell proliferation in leukemia. Consequently, we conjecture that inhibiting PTBP1 activity may be a potential therapeutic strategy for leukemia, which could be validated in future research.

Methods

Cell culture, plasmid construction, and transfection

K562 and 293 T cells were cultured in RPMI 1640 (Gibco, C22400500BT) or DMEM (Gibco, C11995500BT) medium supplemented with 10% FBS (Gibco, 10,099–141 C) and 1% penicillin–streptomycin (Gibco, 15,140,163) at 37 °C in a 5% CO_2 atmosphere, respectively. The cell lines were kindly provided by Prof. Gang Cao from Huazhong Agricultural University, China.

The pcDNA6 plasmid served as a backbone for constructing the minigene reporter and its derivative mutants. Employing human genomic DNA as a template, exons 4–6 of the *SPPL3* gene, along with 500 base pairs of the adjacent intronic sequences, were amplified via PCR using KOD FX polymerase (TOYOBO, KFX-101). The amplified fragments were then seamlessly cloned into the vector. The Basic Seamless Cloning and Assembly Kit (TransGen, CU201-02) facilitated the introduction of point mutations into the minigene (Mt1, Mt2, and Mt3). This was achieved by employing primers that incorporated the desired mutations, allowing for the precise

modification of the minigene sequence. The sequences of primers are shown in Additional file 6: Table S5. MiniGFP was generously provided by Prof. Yang Wang from Dalian Medical University.

The Lipofectamine™ 2000 transfection reagent (ThermoFisher Scientific, 11,668–027) was utilized in conjunction with serum-free medium, opti-MEM (ThermoFisher Scientific, 31,985–070).

RNA extraction and RT-qPCR

A total of 1×10^7 cells were collected and lysed with TRIZOL. Total RNA extraction was performed using the EasyPure Kit (TransGen, ER101-01). Subsequently, 1 μg of RNA was utilized in accordance with the instructions provided by the ABScript II cDNA First-Strand Synthesis Kit (ABclonal, RK20400) for reverse transcription. RT-qPCR was performed on a CFX96 real time PCR machine (Bio-Rad) using SYBR Green Mix. The thermal cycling profile comprised the following steps: 95 °C for 3 min, 40 cycles of 95 °C for 10 s, 56 °C for 20 s and 72 °C for 30 s, followed by a melt curve ranging from 65 to 95 °C with increments of 0.5 °C for 5 s. The sequences of primers are shown in Additional file 6: Table S5.

Western blot

Protein levels were assessed through western blot analysis. Briefly, proteins lysed from cells were separated by SDS-PAGE and subsequently transferred to a PVDF membrane. The PVDF membrane was blocked with non-fat milk powder and incubated with PTBP1 antibody (MBL, RN011P) and β-actin antibody (ABclonal, AC026). Following this, HRP-labeled anti-mouse and anti-rabbit IgG antibodies were employed as secondary antibodies. Protein detection was accomplished using a chemiluminescence system.

RNase R treatment

A total of 1 μg of RNA was subjected to treatment with or without 10 U RNase R (Lucigen, RNR07250) for 50 min at 37 °C in a volume of 10 μL, followed by inactivation at 65 °C for 20 min. An equivalent quantity of untreated RNA served as control for reverse transcription, PCR amplification, and agarose electrophoresis.

CircRNA-seq

A total of 5×10^6 cells were collected for RNA extraction. The removal of rRNA was carried out using the rRNA depletion module (ABclonal, RK20348). RNase R digestion followed the protocol described above, and RNA library construction adhered to the steps outlined in the instructions for the RNA-seq Lib Prep kit for Illumina (ABclonal, RK20303). RNA fragmentation was achieved by adding 5 μL of 2× Frag/Elute buffer. Subsequently, 10 μL of fragmented RNA was combined with RT strand-specific reagent for first-strand synthesis. Following the second-strand synthesis reaction, purification was conducted using AMPure XP magnetic beads (Beckman, A63881). End repair and adapter ligation were followed by another purification step and PCR amplification. RNA sequencing was conducted on an Illumina HiSeq X Ten system, generating paired-end 2× 150 bp reads.

RIP-seq

RIP-seq was conducted following a previously published protocol [42]. A total of 1×10^7 cells were crosslinked with 1% formaldehyde for 10 min at room temperature, and the reaction was halted by adding 2.66 M glycine. The lysed cells were sonicated to fragment DNA into 200–1000 bp fragments. DNase I (ThermoFisher Scientific, EN0521) digestion at 37 °C for 30 min was performed at a concentration of 250 U/mL. Subsequently, 5 μg of antibody was incubated with magnetic beads for 1 h at room temperature. Ten microliters of cell lysate were reserved as control, and the remaining portion was added to the magnetic beads for incubation at 4 °C overnight. Library construction followed the RNA library construction method described above. RNA sequencing was conducted on an Illumina HiSeq X Ten system, generating paired-end 2× 150 bp reads.

CircRNA-seq and RNA-seq analysis

The raw sequencing reads were processed with fastp [43] to remove low-quality reads and adapters. CircRNAs were identified using CIRCexploer2 [44] and CIRIquant [45] software. CIRIquant was used to identify circRNAs by default parameters. During circRNA identification with CIRCexplorer2, cleaned reads were mapped to the hg38 reference genome by STAR [46] with specific parameters: –chimSegmentMin 10 –readFilesCommand zcat –outSAMtype BAM SortedByCoordinate. CircRNAs identified by both software were subjected to further analysis. The junction ratio was calculated by CIRIquant using back splicing junction (BSJ) and forward splicing junction (FSJ) reads as 2 * BSJ/(2 * BSJ + FSJ). To compare circRNA expression level between samples, circRNA BSJ counts was normalized using the CPM (counts per million mapped reads) to remove bias derived from sequencing depth. Differentially expressed circRNAs were identified using edgeR [47] with a threshold: $\log_2|FC| > 1$ and p value < 0.05. ggplot2 R package was employed to generate relevant plots.

RNA-seq reads were aligned to the hg38 reference genome using HISAT2 [48]. Gene expression levels were quantified using StringTie [49] with the specified parameters -e -G Homo_sapiens.GRCh38.96.gtf, and

differentially expressed genes were identified through DESeq2 [50] with a threshold of $\log_2$ |FC|> 2 and p value < 0.05.

To explore circRNA expression after PTBP1 knockdown in other cells, RNA-seq and circRNA-seq data for the CD34 + and HeLa cells were downloaded from GSE106566 [51] and CRA001838 datasets (https://bigd.big.ac.cn/gsa) [45], respectively. Additionally, RNA-seq data for AML and healthy tissues were obtained from GSE158596 [52] to investigate for the relationship between PTBP1 and circRNAs in AML and construct the ceRNA regulatory network.

CircRNA co-expression network construction

After obtaining circRNA expression from 10 cell lines in the ENCODE project, the rcorr function of the Hmisc R package (https://www.rdocumentation.org/packages/Hmisc/versions/5.1-2) was used to calculate the Pearson correlation coefficients for each pair of circRNAs across 10 cell lines. To improve the accuracy, circRNAs with CPM ≥ 0.2 in at least one cell line and Pearson correlation coefficient > 0.9 were selected to construct co-expression networks.

Analysis for RBP motifs in circRNA flanking introns

Long nonpolyA RNA-seq data of 10 cell lines, including K562, A549, HeLaS3, and HepG2, were obtained from the ENCODE project [53] (download link: http://hgdownload.cse.ucsc.edu/goldenPath/hg19/encodeDCC/wgEncodeCshlLongRnaSeq/). After circRNA identification in 10 cell lines, to collect reliable RBP resources, the RBP position weight matrices (PWMs) present both in CISBP-RNA [54] and RBPsuite [55] databases were obtained for subsequent analysis. MEME-FIMO [56] was employed to scan RBP motifs in the sequences of circRNA flanking introns with p value < 0.0001.

RIP-seq analysis

After aligning the cleaned reads to the human reference genome hg38 by HISAT2, the low mapping quality reads were filtered with -q 30 using SAMtools [57], and PCR duplicates were subsequently removed using picard (https://github.com/broadinstitute/picard). MACS2 software [58] was performed to call peaks with parameter: -f BAMPE -B -g hs, and genomic region annotations of peaks were conducted using ChIPseeker [59] (promoter defined as transcription start site ± 2 kb). Additionally, visualization files in bw format were generated using deepTools [60] bamCoverage (–normalizeUsing RPGC, –bin size 10). Subsequently, motif enrichment analysis of PTBP1 peaks was performed using HOMER [61] with the parameters (findMotifGenome.pl: -len 6).

CeRNA network construction

The differentially expressed circRNAs in AML were scanned with MEME-FIMO with p value < 0.0001, and the circRNAs with PTBP1 motif in flanking introns or body were used for ceRNA network analysis. Potential miRNAs binding to these circRNAs were predicted using Miranda [62], with stringent parameters: score > 200, E < −7, and -strict. Subsequently, miRNA-mRNA interactions were predicted by TargetScan [63], and the results overlapping with miRTarBase [64] database, which stores experimentally validated miRNA-mRNA interactions, were remained. The results were filtered based on circRNAs having the same expression trend as the target differentially expressed genes. Six upregulated hub circRNAs related to cell proliferation were selected for presentation.

Gene function enrichment analysis

The results of differentially expressed genes in AML were filtered based on p value < 0.05. After sorting these genes based on $\log_2$ fold change, the gene set enrichment analysis (GSEA) was employed to examine the enrichment of genes in pathways related to proliferation, migration, and mRNA splice site selection using the enrichplot R package [65]. Additionally, differentially expressed genes in the constructed ceRNA network were subjected to GO and KEGG enrichment analyses using DAVID database [66]. Relevant figures were visualized using circlize [67] and xenrichplot packages.

Statistical analysis

Except specifically labeled, data are presented as the mean of three biological replicates, error bars represent the mean ± standard error of mean (SEM), and statistical significance was performed using Student's t-test (two-tailed, unpaired): ns, no significant difference, * $p < 0.05$, ** $p < 0.01$, *** $p < 0.001$, **** $p < 0.0001$.

Abbreviations

circRNAs	Circular RNAs
ceRNA	Competitive endogenous RNA
AML	Acute myeloid leukemia
RCMs	Reverse complementary matches
RBPs	RNA binding proteins
GSEA	Gene set enrichment analysis
GO	Gene ontology
BSJ	Back splicing junction
FSJ	Forward splicing junction

Supplementary Information

The online version contains supplementary material available at https://doi.org/10.1186/s12915-025-02233-8.

Additional File 1: Figures S1-S5. FigS1. Validation of PTBP1 knockdown cell lines. FigS2. Expression of differentially expressed circRNAs and corresponding linear mRNAs after PTBP1 knockdownin K562 cells. FigS3. Expression of differentially expressed circRNAs and linear mRNAs after

knockdown of PTBP1 in different cells. FigS4. Characterization and validation of circ*SPPL3*. FigS5. The features of differentially expressed circRNAs in AML.

Additional File 2: Tables S1. CircRNAs identified from CIRIquant and CIRCexplorer2

Additional File 3: Tables S2. Expression levels of circRNA co-identified using CIRIquant and CIRCexplorer2 in K562 cell line

Additional File 4: Tables S3. Differentially expressed circRNAs from WT-shP1 and WT-shP2 in K562 cell line

Additional File 5: Tables S4. Differentially expressed genes from WT-shP1 and WT-shP2 in K562 cell line

Additional File 6: Tables S5. Primers used for validation

Additional File 7: Tables S6. Junction ratio of 49 overlapping differentially expressed circRNAs in K562 cell line

Additional File 8: Tables S7. CeRNA network of 6 hub circRNAs

Additional File 9: Original gels and blots images

Acknowledgements
We thank Prof. Yang Wang and Dr. Yangfan Qi (Dalian Medical University, China) for sharing a miniGFP plasmid. We thank Ms. Hongzhen Gao for her thesis as an important reference to this study.

Authors'contribution
Conception and design: G.L., and M.W.; Data generation: M.W., and S.Z. with the assistance of Y.Z., and J.Z.; Data analysis: S.Z., M.W., J.Z., and F.L.; Data interpretation and paper writing: M.W., S.Z., Y.Z., F.L., C.Z., Q.Z., X.L., and G.L.; All authors read and approved the final manuscript.

Funding
This work was supported by the National Natural Science Foundation of China (32370630, 32250710678), and the National Key Research and Development Program of China (2021YFC2701201).

Data availability
The RNA-seq, circRNA-seq and PTBP1 RIP-seq data generated in this project for K562 cell line have been deposited in the Genome Sequence Archive [68] in National Genomics Data Centre [69], China National Center for Bioinformation/Beijing Institute of Genomics, Chinese Academy of Sciences (GSA-Human: HRA006344) that are publicly accessible at https://bigd.big.ac.cn/gsa-human (Shared URL: https://ngdc.cncb.ac.cn/gsa-human/browse/HRA006344) [70]. RNA-seq and circRNA-seq data for the CD34+ and HeLa cells were downloaded from GSE106566 (https://www.ncbi.nlm.nih.gov/geo/query/acc.cgi?acc=GSE106566) [51] and CRA001838 datasets (https://ngdc.cncb.ac.cn/gsa/browse/CRA001838) [45], respectively. RNA-seq data for AML and healthy tissues were obtained from GSE158596 (https://www.ncbi.nlm.nih.gov/geo/query/acc.cgi?acc=GSE158596) [52].

Declarations

Ethics approval and consent to participate
Not applicable.

Consent for publication
Not applicable.

Competing interests
The authors declare no competing interests.

Author details
[1]National Key Laboratory of Crop Genetic Improvement, Hubei Hongshan Laboratory, Huazhong Agricultural University, Wuhan 430070, China. [2]Agricultural Bioinformatics Key Laboratory of Hubei Province, Hubei Engineering Technology Research Center of Agricultural Big Data, Key Laboratory of Smart Farming Technology for Agricultural Animals, 3D Genomics Research Center, College of Informatics, Huazhong Agricultural University, Wuhan 430070, China.

Received: 27 May 2024 Accepted: 2 May 2025
Published online: 12 May 2025

References

1. Capel B, Swain A, Nicolis S, Hacker A, Walter M, Koopman P, Goodfellow P, Lovell-Badge R. Circular transcripts of the testis-determining gene Sry in adult mouse testis. Cell. 1993;73:1019–30.
2. Cocquerelle C, Mascrez B, Hétuin D, Bailleul B. Mis-splicing yields circular RNA molecules. Faseb j. 1993;7:155–60.
3. Aktaş T, Avşar Ilık İ, Maticzka D, Bhardwaj V, Pessoa Rodrigues C, Mittler G, Manke T, Backofen R, Akhtar A. DHX9 suppresses RNA processing defects originating from the Alu invasion of the human genome. Nature. 2017;544:115–9.
4. Liu CX, Chen LL. Circular RNAs: characterization, cellular roles, and applications. Cell. 2022;185:2016–34.
5. Bosson AD, Zamudio JR, Sharp PA. Endogenous miRNA and target concentrations determine susceptibility to potential ceRNA competition. Mol Cell. 2014;56:347–59.
6. Tay Y, Rinn J, Pandolfi PP. The multilayered complexity of ceRNA crosstalk and competition. Nature. 2014;505:344–352.
7. Chen LL. The biogenesis and emerging roles of circular RNAs. Nat Rev Mol Cell Biol. 2016;17:205–11.
8. Xia B, Hong T, He X, Hu X, Gao Y. A circular RNA derived from MMP9 facilitates oral squamous cell carcinoma metastasis through regulation of MMP9 mRNA stability. Cell Transplant. 2019;28:1614–23.
9. Yoshimoto R, Rahimi K, Hansen TB, Kjems J, Mayeda A. Biosynthesis of circular RNA ciRS-7/CDR1as is mediated by mammalian-wide interspersed repeats. iScience. 2020;23:101345.
10. Conn SJ, Pillman KA, Toubia J, Conn VM, Salmanidis M, Phillips CA, Roslan S, Schreiber AW, Gregory PA, Goodall GJ. The RNA binding protein quaking regulates formation of circRNAs. Cell. 2015;160:1125–34.
11. Ashwal-Fluss R, Meyer M, Pamudurti NR, Ivanov A, Bartok O, Hanan M, Evantal N, Memczak S, Rajewsky N, Kadener S. circRNA biogenesis competes with pre-mRNA splicing. Mol Cell. 2014;56:55–66.
12. Errichelli L, Dini Modigliani S, Laneve P, Colantoni A, Legnini I, Capauto D, Rosa A, De Santis R, Scarfò R, Peruzzi G, et al. FUS affects circular RNA expression in murine embryonic stem cell-derived motor neurons. Nat Commun. 2017;8:14741.
13. Knupp D, Cooper DA, Saito Y, Darnell RB, Miura P. NOVA2 regulates neural circRNA biogenesis. Nucleic Acids Res. 2021;49:6849–62.
14. Shen H, An O, Ren X, Song Y, Tang SJ, Ke XY, Han J, Tay DJT, Ng VHE, Molias FB, et al. ADARs act as potent regulators of circular transcriptome in cancer. Nat Commun. 2022;13:1508.
15. Ho JS, Di Tullio F, Schwarz M, Low D, Incarnato D, Gay F, Tabaglio T, Zhang J, Wollmann H, Chen L, et al. HNRNPM controls circRNA biogenesis and splicing fidelity to sustain cancer cell fitness. Elife. 2021;10: e59654.
16. Fei T, Chen Y, Xiao T, Li W, Cato L, Zhang P, Cotter MB, Bowden M, Lis RT, Zhao SG, et al. Genome-wide CRISPR screen identifies HNRNPL as a prostate cancer dependency regulating RNA splicing. Proc Natl Acad Sci U S A. 2017;114:E5207–15.
17. Xue Y, Zhou Y, Wu T, Zhu T, Ji X, Kwon YS, Zhang C, Yeo G, Black DL, Sun H, et al. Genome-wide analysis of PTB-RNA interactions reveals a strategy used by the general splicing repressor to modulate exon inclusion or skipping. Mol Cell. 2009;36:996–1006.
18. Pérez I, Lin CH, McAfee JG, Patton JG. Mutation of PTB binding sites causes misregulation of alternative 3′ splice site selection in vivo. RNA. 1997;3:764–78.
19. Qi Y, Han W, Chen D, Zhao J, Bai L, Huang F, Dai Z, Li G, Chen C, Zhang W, et al. Engineering circular RNA regulators to specifically promote circular RNA production. Theranostics. 2021;11:7322–36.
20. Chu Z, Zhu M, Luo Y, Hu Y, Feng X, Wang H, Sunagawa M, Liu Y. PTBP1 plays an important role in the development of gastric cancer. Cancer Cell Int. 2023;23:195.
21. Zeng H, Chen W, Zheng R, Zhang S, Ji JS, Zou X, Xia C, Sun K, Yang Z, Li H, et al. Changing cancer survival in China during 2003–15: a pooled analysis of 17 population-based cancer registries. Lancet Glob Health. 2018;6:e555–67.
22. Liu P, Gao S, Li Z, Pan S, Luo G, Ji Z. Endothelial progenitor cell-derived exosomes inhibit pulmonary artery smooth muscle cell in vitro

proliferation and resistance to apoptosis by modulating the Mitofusin-2 and Ras-Raf-ERK1/2 signaling pathway. Eur J Pharmacol. 2023;949: 175725.
23. Sun Y, Liu WZ, Liu T, Feng X, Yang N, Zhou HF. Signaling pathway of MAPK/ERK in cell proliferation, differentiation, migration, senescence and apoptosis. J Recept Signal Transduct Res. 2015;35:600–4.
24. Zhang M, Zhang X. The role of PI3K/AKT/FOXO signaling in psoriasis. Arch Dermatol Res. 2019;311:83–91.
25. Zhang N, Liu Z, Lai X, Liu S, Wang Y. Silencing of CD147 inhibits cell proliferation, migration, invasion, lipid metabolism dysregulation and promotes apoptosis in lung adenocarcinoma via blocking the Rap1 signaling pathway. Respir Res. 2023;24:253.
26. Zhang Y, Alexander PB, Wang XF. TGF-β family signaling in the control of cell proliferation and survival. Cold Spring Harb Perspect Biol. 2017;9: a022145.
27. Zhang QX, Pan YM, Xiao HL, An N, Deng SS, Du X. Alternative splicing analysis showed the splicing factor polypyrimidine tract-binding protein 1 as a potential target in acute myeloid leukemia therapy. Neoplasma. 2022;69:1198–208.
28. Ziegler N, Cortés-López M, Alt F, Sprang M, Ustjanzew A, Lehmann N, El Malki K, Wingerter A, Russo A, Beck O, et al. Analysis of RBP expression and binding sites identifies PTBP1 as a regulator of CD19 expression in B-ALL. Oncoimmunology. 2023;12:2184143.
29. Zhang J, Hou L, Zuo Z, Ji P, Zhang X, Xue Y, Zhao F. Comprehensive profiling of circular RNAs with nanopore sequencing and CIRI-long. Nat Biotechnol. 2021;39:836–45.
30. Haque S, Ames RM, Moore K, Lee BP, Jeffery N, Harries LW. Islet-expressed circular RNAs are associated with type 2 diabetes status in human primary islets and in peripheral blood. BMC Med Genomics. 2020;13:64.
31. Wu B, Chen X, Pan X, Deng X, Li S, Wang Z, Wang J, Liao D, Xu J, Chen M, et al. Single-cell transcriptome analyses reveal critical roles of RNA splicing during leukemia progression. PLoS Biol. 2023;21: e3002088.
32. Yoshimi A, Lin KT, Wiseman DH, Rahman MA, Pastore A, Wang B, Lee SC, Micol JB, Zhang XJ, de Botton S, et al. Coordinated alterations in RNA splicing and epigenetic regulation drive leukaemogenesis. Nature. 2019;574:273–7.
33. Luo G, Li R, Li Z. CircRNA circFNDC3B promotes esophageal cancer progression via cell proliferation, apoptosis, and migration regulation. Int J Clin Exp Pathol. 2018;11:4188–96.
34. Wang L, Tan Y, Chen J, Zhu Z, Zhu Y, Sun Q, Dong H, Ai C, He G, Liu Y. CircABCC1 promotes the development of glioma by sponging miR-591 and modulating high-mobility group A2. Ann N Y Acad Sci. 2022;1511:107–18.
35. Wang K, Wang N, Liu J, Zhou J, Lei S, Yue H, Feng H, Feng K, Kang X. Silencing circular RNA hsa_circABCC1 inhibits osteosarcoma progression through down-regulating HDAC4 via sponging miR-591. Environ Toxicol. 2023;38:1565–76.
36. Zhang R, Li Y, Wang H, Zhu K, Zhang G. The regulation of circRNA RNF13/miRNA-1224-5p axis promotes the malignant evolution in acute myeloid leukemia. Biomed Res Int. 2020;2020:5654380.
37. Chen Y, Li S, Wei Y, Xu Z, Wu X. Circ-RNF13, as an oncogene, regulates malignant progression of HBV-associated hepatocellular carcinoma cells and HBV infection through ceRNA pathway of circ-RNF13/miR-424-5p/TGIF2. Bosn J Basic Med Sci. 2021;21:555–68.
38. Mo Y, Wang Y, Zhang S, Xiong F, Yan Q, Jiang X, Deng X, Wang Y, Fan C, Tang L, et al. Circular RNA circRNF13 inhibits proliferation and metastasis of nasopharyngeal carcinoma via SUMO2. Mol Cancer. 2021;20:112.
39. Zhu Z, Mo S, Wang X, Meng M, Qiao L. Circ-AGTPBP1 promotes white matter injury through miR-140-3p/Pcdh17 axis role of Circ-AGTPBP1 in white matter injury. J Bioenerg Biomembr. 2023;56:1–14.
40. Khamphaya T, Chukijrungroat N, Saengsirisuwan V, Mitchell-Richards KA, Robert ME, Mennone A, Ananthanarayanan M, Nathanson MH, Weerachayaphorn J. Nonalcoholic fatty liver disease impairs expression of the type II inositol 1,4,5-trisphosphate receptor. Hepatology. 2018;67:560–74.
41. Zhai X, Chen X, Wan Z, Ge M, Ding Y, Gu J, Hua J, Guo D, Tan M, Xu D. Identification of the novel therapeutic targets and biomarkers associated of prostate cancer with cancer-associated fibroblasts (CAFs). Front Oncol. 2023;13:1136835.
42. Gagliardi M, Matarazzo MRRIP. RNA immunoprecipitation. Methods Mol Biol. 2016;1480:73–86.
43. Chen S, Zhou Y, Chen Y, Gu J. fastp: an ultra-fast all-in-one FASTQ preprocessor. Bioinformatics. 2018;34:i884–90.
44. Zhang XO, Dong R, Zhang Y, Zhang JL, Luo Z, Zhang J, Chen LL, Yang L. Diverse alternative back-splicing and alternative splicing landscape of circular RNAs. Genome Res. 2016;26:1277–87.
45. Zhang J, Chen S, Yang J, Zhao F. Accurate quantification of circular RNAs identifies extensive circular isoform switching events. Nat Commun. 2020;11:90.
46. Dobin A, Gingeras TR. Mapping RNA-seq reads with STAR. Curr Protoc Bioinformatics. 2015;51:11.14.11–11.14.19.
47. Robinson MD, McCarthy DJ, Smyth GK. edgeR: a Bioconductor package for differential expression analysis of digital gene expression data. Bioinformatics. 2010;26:139–40.
48. Pertea M, Kim D, Pertea GM, Leek JT, Salzberg SL. Transcript-level expression analysis of RNA-seq experiments with HISAT. StringTie and Ballgown Nat Protoc. 2016;11:1650–67.
49. Pertea M, Pertea GM, Antonescu CM, Chang TC, Mendell JT, Salzberg SL. StringTie enables improved reconstruction of a transcriptome from RNA-seq reads. Nat Biotechnol. 2015;33:290–5.
50. Love MI, Huber W, Anders S. Moderated estimation of fold change and dispersion for RNA-seq data with DESeq2. Genome Biol. 2014;15:550.
51. Liu J, Li Y, Tong J, Gao J, Guo Q, Zhang L, Wang B, Zhao H, Wang H, Jiang E, et al. Long non-coding RNA-dependent mechanism to regulate heme biosynthesis and erythrocyte development. Nat Commun. 2018;9:4386.
52. Lux S, Blätte TJ, Gillissen B, Richter A, Cocciardi S, Skambraks S, Schwarz K, Schrezenmeier H, Döhner H, Döhner K, et al. Deregulated expression of circular RNAs in acute myeloid leukemia. Blood Adv. 2021;5:1490–503.
53. ENCODE Project Consortium. An integrated encyclopedia of DNA elements in the human genome. Nature. 2012;489:57–74.
54. Ray D, Kazan H, Cook KB, Weirauch MT, Najafabadi HS, Li X, Gueroussov S, Albu M, Zheng H, Yang A, et al. A compendium of RNA-binding motifs for decoding gene regulation. Nature. 2013;499:172–7.
55. Pan X, Fang Y, Li X, Yang Y, Shen HB. RBPsuite: RNA-protein binding sites prediction suite based on deep learning. BMC Genomics. 2020;21:884.
56. Grant CE, Bailey TL, Noble WS. FIMO: scanning for occurrences of a given motif. Bioinformatics. 2011;27:1017–8.
57. Li H, Handsaker B, Wysoker A, Fennell T, Ruan J, Homer N, Marth G, Abecasis G, Durbin R. The Sequence Alignment/Map format and SAMtools. Bioinformatics. 2009;25:2078–9.
58. Zhang Y, Liu T, Meyer CA, Eeckhoute J, Johnson DS, Bernstein BE, Nusbaum C, Myers RM, Brown M, Li W, et al. Model-based analysis of ChIP-Seq (MACS). Genome Biol. 2008;9:R137.
59. Yu G, Wang LG, He QY. ChIPseeker: an R/Bioconductor package for ChIP peak annotation, comparison and visualization. Bioinformatics. 2015;31:2382–3.
60. Ramirez F, Dundar F, Diehl S, Gruning BA, Manke T. deepTools: a flexible platform for exploring deep-sequencing data. Nucleic Acids Res. 2014;42:W187–191.
61. Heinz S, Benner C, Spann N, Bertolino E, Lin YC, Laslo P, Cheng JX, Murre C, Singh H, Glass CK. Simple combinations of lineage-determining transcription factors prime cis-regulatory elements required for macrophage and B cell identities. Mol Cell. 2010;38:576–89.
62. Enright AJ, John B, Gaul U, Tuschl T, Sander C, Marks DS. MicroRNA targets in Drosophila. Genome Biol. 2003;5:R1.
63. Agarwal V, Bell GW, Nam JW, Bartel DP. Predicting effective microRNA target sites in mammalian mRNAs. Elife. 2015;4: e05005.
64. Huang HY, Lin YC, Cui S, Huang Y, Tang Y, Xu J, Bao J, Li Y, Wen J, Zuo H, et al. miRTarBase update 2022: an informative resource for experimentally validated miRNA-target interactions. Nucleic Acids Res. 2022;50:D222–30.
65. Wu T, Hu E, Xu S, Chen M, Guo P, Dai Z, Feng T, Zhou L, Tang W, Zhan L *et al*. clusterProfiler 4.0: a universal enrichment tool for interpreting omics data. Innovation (Camb). 2021;2:100141.
66. Sherman BT, Hao M, Qiu J, Jiao X, Baseler MW, Lane HC, Imamichi T, Chang W. DAVID: a web server for functional enrichment analysis and functional annotation of gene lists (2021 update). Nucleic Acids Res. 2022;50:W216–21.
67. Gu Z, Gu L, Eils R, Schlesner M, Brors B. circlize implements and enhances circular visualization in R. Bioinformatics. 2014;30:2811–2.
68. Chen T, Chen X, Zhang S, Zhu J, Tang B, Wang A, Dong L, Zhang Z, Yu C, Sun Y, et al. The genome sequence archive family: toward explosive data growth and diverse data types. Genomics Proteomics Bioinformatics. 2021;19:578–83.

69. CNCB-NGDC Members and Partners. Database resources of the National Genomics Data Center, China National Center for Bioinformation in 2022. Nucleic Acids Res. 2022;50:D27–38.
70. Li G. PTBP1 regulates circRNA biogenesis in leukaemia. Transcriptome analysis. NGDC GSA-Human Bioproject https://ngdc.cncb.ac.cn/gsa-human/browse/HRA006344 (2025).

Publisher's Note